Main Manuscript for

Translational regulation enhances distinction of cell types in the nervous system

Authors:

Toshiharu Ichinose[1,2,*], Shu Kondo[3], Mai Kanno[2], Yuichi Shichino[4], Mari Mito[4], Shintaro Iwasaki[4,5], Hiromu Tanimoto[2,*].

Affiliations:

1: Frontier Research Institute for Interdisciplinary Sciences, Tohoku University; 2: Graduate School of Life Sciences, Tohoku University; 3: Faculty of Advanced Engineering, Tokyo University of Sciences; 4: RNA Systems Biochemistry Laboratory, RIKEN Cluster for Pioneering Research, Wako, Saitama 351-0198, Japan 5: Department of Computational Biology and Medical Sciences, Graduate School of Frontier Sciences, The University of Tokyo, Kashiwa, Chiba 277-8561, Japan.

Correspondence authors:

Hiromu Tanimoto (hiromut@m.tohoku.ac.jp) and Toshiharu Ichinose (toshiharu.ichinose.c1@tohoku.ac.jp)

Author Contributions:

TI, SK, and HT conceptualized the project; TI performed ribosome profiling and RNA-seq with the help of YS, MM, and SI; MK performed immunohistochemistry and fluorescent in-situ hybridization, and managed fly care; SK constructed the transgenic reporter strain; YS, MM, and SI contributed to reagents, protocols, and analytic tools; TI analyzed all data with the help of YS and SI; TI and HT wrote the manuscript; SK, YS and SI edited the manuscript.

Competing Interest Statement:

The authors declare no competing interest.

Classification:

BIOLOGICAL SCIENCES, Neuroscience

Keywords:

Cellular heterogeneity, Translational regulation, Drosophila nervous system

This PDF file includes:

Main Text

Figures 1 to 5

Abstract:

Multicellular organisms are composed of specialized cells with distinct proteomes. While recent advances in single-cell transcriptome analyses have revealed differential expression of mRNAs, cellular diversity in translational profiles remains to be understood. By performing RNA-seq and Ribo-seq from genetically labelled cell types in *Drosophila*, we profiled the transcriptome and translatome of neuronal and glial cells in the brain. This comparative profiling revealed substantial posttranscriptional regulation of protein expression. We further found that translational efficiency of proteins fundamental to neuronal functions, such as ion channels and neurotransmitter receptors, was maintained low especially in glia, leading to preferential translation in neurons. Notably, the distribution of ribosome footprints on these mRNAs exhibited a remarkable bias towards the 5′ untranslated regions (UTR) in glial cells. Using a transgenic reporter system, we provide evidence that the UTR confer translational suppression selectively in glia. Overall, these findings underscore the profound impact of translational regulation in shaping cell identity and provide new insights into the molecular mechanisms driving cell-type diversity.

Significance Statement:

Despite sharing the same genome, diverse cell types in our body exhibit distinct functions and morphologies. This cellular diversity arises from the synthesis of differential sets of proteins. While transcriptional controls of gene expression have been extensively studied, the role of translational regulations in cell-type specialization remains underinvestigated. Here, we examined the contribution of these two steps to cellular heterogeneity in the fruit fly brain by comparing mRNA expression (transcriptome) and ribosome distribution on mRNA (translatome). Our dataset provides compelling evidence that cell-type distinctions in the transcriptomes are further augmented at the level of mRNA translation. Our findings thus shed light on the previously unexplored role of translational regulations in shaping cell type diversity.

58 **Introduction:**

59 Gene expression is heavily regulated both at the transcription and translation levels (1–
60 5), and its heterogeneity defines the specialized morphologies and functions of cells. The
61 *Drosophila* brain is a well-studied model tissue containing more than 5,000 morphologically
62 distinct cell types (6). Recent advances in single-cell transcriptomics have identified groups of
63 differentially expressed genes and provided an in-depth overview of cellular diversity in the
64 transcriptomes (7–9). On the other hand, translational regulations in cell-type specialization
65 remain to be elucidated.

66 The two major cell types in the brain, neuronal and glial cells, have distinct physiological
67 functions. Neurons are specialized for synaptic and electric communication with high targeted
68 specificity, temporal precision, and long distance. In contrast, glial cells form the blood brain
69 barrier, maintain homeostasis of extracellular ion, nutrition, and neurotransmitters, and act as
70 immune cells (10). Despite these clear differences, the transcriptomes of neurons and glia
71 share similarity according to recent single-cell transcriptome analyses (7–9), suggesting
72 substantial post-transcriptional processes to distinguish their proteomes.

73 Ribosome profiling or Ribo-seq, which is based on deep-sequencing of mRNA fragments
74 protected by ribosomes from RNase treatment (ribosome footprints), has been a powerful
75 approach to provide a genome-wide snapshot of protein synthesis ('translatome') (11).
76 Application of this method, combined with transcriptome analysis, revealed multiple layers of
77 translational regulation in cells. For example, this comparison allowed measurements of
78 translational efficiency (TE), which is quantified as the number of ribosome footprints on the
79 coding sequence per mRNA, and discoveries of previously unannotated ORFs (11–14). While
80 TE profiles have been reported to be variable among dissected animal tissues (13,15,16),
81 differences in translational regulations among identified cell types remain unclear.

82 Here, we examine the comprehensive landscape of translational profiles between
83 neuronal and glial cells in the *Drosophila* head. Due to the size of the fly brain (~0.5 mm) and
84 intricate intercellular adhesions among neurons and glia (17), surgical separation is
85 impractical. We thus biochemically purified ribosome-bound mRNAs through genetic tagging
86 of ribosomes in target cells (18–22) and further performed Ribo-seq and RNA-seq. By this
87 comparative transcriptome-translatome analyses, we suggest that differential translational
88 programs enhance the distinction of protein synthesis between neuronal and glial cells.

89

90 **Results:**

91 **Comparative transcriptome-translatome analyses reveal translational suppression of**
92 **selective groups of proteins in the fly heads**

93 To gain an overview of the translation status, we first applied conventional Ribo-seq in the
94 whole fly head, and successfully monitored footprint distribution at a single-codon resolution
95 (Figure 1A, see *Materials and Methods* for technical details). The majority (96.2%) of ribosome
96 footprints were mapped onto the annotated coding sequences (CDS), and its distribution
97 displayed a clear 3-nt periodicity, reflecting the codon-wise movement (Figure 1B).

98 To compare transcriptome and translatome, we also performed RNA-seq from the same
99 lysate (Figure 1A). As previously reported, the transcript level and the number of ribosome
100 footprints did not always match, suggesting substantial post-transcriptional regulations (R^2 =
101 0.664; Figure 1C). For instance, while *Shaker* (*Sh*) and *Trehalase* (*Treh*), which encode a
102 voltage-gated K^+ channel and an enzyme that hydrolyzes trehalose, respectively, were similar
103 regarding transcript levels, far more ribosome footprints were detected on *Treh* (Figure 1D-E).
104 We therefore measured translational efficiency (TE), ribosome footprints normalized by mRNA
105 reads. TE was much higher for *Treh* than *Sh* (Figure 1F), and we found a striking genome-
106 wide variability with more than 20-fold TE difference between the 5 and 95 percentiles (Figure
107 1G). Kyoto Encyclopedia of Genes and Genome (KEGG) pathway enrichment analysis
108 revealed that transcripts involved in fatty acid metabolism and proteasome are actively
109 translated (Figure 1H). In contrast, ribosome proteins, as previously reported (18,23), and
110 proteins mediating neuronal ligand-receptor interactions were significantly enriched in the
111 transcripts with low TE, suggesting translational suppression (Figure 1H). Indeed, many
112 transcripts encoding ligand- or voltage-gated ion channels, G-protein coupled receptors
113 (GPCR) showed remarkably low TE (Figure 1C and 1I). These results suggest translational
114 regulations specific to neuronal transcripts in the fly head.

115 **Translational regulation enhances the difference of the gene expression profiles**
116 **between cell types**

117 Because the translatome/transcriptome status of the whole heads was a mixed average
118 of diverse cell types, such as neurons, glial cells, fat bodies, and muscles, we set up an
119 experimental approach to dissect cell-type specific translational regulations. By expressing
120 epitope-tagged RpL3 (uL3 in universal nomenclature) (18) under the control of UAS using the
121 *nSyb*- or the *repo*- GAL4 drivers, we immunopurified the tagged ribosomes and associated

122 mRNAs separately from neurons and glia, and performed Ribo-seq (Figure 2A). By
123 immunohistochemistry, we confirmed that *UAS-RpL3::FLAG* on the third chromosome
124 exhibited minimum leakage expression in the brain and did not display any apparent
125 morphological defects upon expression using either driver, compared to other insertions or
126 constructs (18,22,24) (Figures 2A and S1A-B). By the purification of FLAG-tagged ribosomes,
127 we successfully profiled translatome from neurons and glial cells in the fly heads: Footprints
128 were found on 10,821 (78.4 % of all the annotated genes) and 10,994 (79.7 %) genes in
129 neurons and glia, respectively, with decent reproducibility among the biological replicates (R^2
130 > 0.9, Figure S1C). The known marker genes were strongly enriched while non-target markers
131 were depleted (Figures 2B and S1D-E) (7–9), and the KEGG enrichment analysis showed
132 significant enrichment of footprints on genes associated with the known functions of these cell
133 types (Figure S1F). Interestingly, the KEGG analysis also revealed that neurons exhibit a
134 greater extent of protein synthesis related to oxidative phosphorylation and mitochondrial
135 ribosome proteins, while glial cells show higher expression of proteins associated with
136 glycolysis (Figure S1F-G). These findings support the glia-neuron lactate shuttle hypothesis,
137 a recently proposed concept of metabolic specialization (25,26). Furthermore, apart from the
138 annotated CDS, we detected clustered ribosome footprints on *Hsr-ω*, previously annotated as
139 a long non-coding RNA, strongly suggesting the synthesis of hitherto undescribed
140 polypeptides (Figure S1H) (27). Altogether, the combination of genetic labelling of ribosomes
141 in selective cell types and Ribo-seq revealed the differential translatome profiles in the fly
142 heads.

143 To further examine translational regulation, we performed RNA-seq from the same
144 immunoprecipitated lysates (Figures 2A, S2A-B) and calculated TE in neuronal and glial cells.
145 Because our approach relies on the ribosome-mRNA complex, we may miss mRNA with little
146 translational activity, potentially leading to underestimation for such transcripts. Nevertheless,
147 we identified groups of genes undergoing neuron- or glia- specific translational regulations
148 compared to the whole heads (Figure S3A). Genes mediating fatty acid metabolism and
149 degradation, for example, were actively translated in the whole head, but showed lower TE in
150 neurons or in glia (Figures 1H and 2C). Because many of these genes are highly expressed
151 in the fat bodies (28,29), these results suggest selective translational enhancement in the fat
152 body. Strikingly, TE of genes involved in neuroactive ligand-receptor interaction was
153 significantly higher in neurons but lower in glia (Figure 2C-D), suggesting cell-type specific
154 translational regulation of these genes.

155 This differential translational regulation was highlighted in weak TE correlation between
156 neurons and glia (R^2 = 0.534, Figure 2E). We found that genes transcribed less in glia tend to
157 be further suppressed at translation (Figure 2F). Specifically, many functionally-characterized
158 neuronal genes, such as voltage- or ligand- gated ion channels, G-protein coupled receptors,
159 neuropeptides and proteins for visual perception, showed particularly lower TE in glia (Figures
160 2E, 2G and S3B). For these genes, the distinction between neuronal and glial cells was much
161 exaggerated at the level of translation than at transcription (Figure 2H). Consistently on the
162 genome-wide sacle, the inter-cell type correlation was weaker in translatome compared to in
163 transcriptome (R^2 = 0.59 vs. 0.81, Figure S3C). These data together indicate substantial
164 contributions of translational regulation to shaping the cell-type identities.

165 **Biased distribution of ribosomes to upstream open reading frames of neural genes in**
166 **glial cells**

167 We next analyzed the distribution of ribosome footprints on the differentially translated
168 transcripts (DTT). Fat-body related genes showed lower TE in neurons compared to the whole
169 head (Figure 2C). Among these genes, we found a remarkable ribosome accumulation on the
170 start codon specifically in neurons (Figure S4), as if the first round of the elongation cycle was
171 arrested in neurons. On the other hand, DTTs suppressed in glial cells compared to neurons
172 (defined as genes with more than 10 times higher TE in neurons than in glia, n = 161), we
173 noticed that glial ribosome footprints were remarkably biased towards 5′ UTR (Figure 3A-B).
174 Notably, this pattern was not obvious on the genome-wide scale (Figure 3A-B). The high
175 5′UTR/CDS ratio of ribosome footprints in glia was commonly observed on many transcripts
176 with known neuronal functions, such as *Rab3, Syt4, Arr1* and *Syn* (Figure 3D-E). These results
177 suggest that glial cells suppress the synthesis of neuronal proteins by shifting the ribosome
178 affinity to the 5′ UTR.

179 We reasoned translational downregulation via upstream open reading frames (uORFs) in
180 the 5′ UTR, as the translation of uORFs was reported to suppress that of the downstream main
181 ORF (13,30,31). Consistent with this idea, metagene plot around the AUG codons on 5′ UTR
182 in glia revealed strong accumulation of footprints on the upstream AUG codons, similar to
183 those observed on the initiation codon of CDSs (Figures 4A-B). We calculated the footprint
184 accumulation score on each codon (defined as the ratio of footprints on each codon with
185 surrounding -50/+50 nt), and found that AUG and the near cognate codons (NUG or AUN)
186 showed relatively high accumulation (Figure 4C). On the other hand, any codons did not exhibit
187 the significant accumulation inside the annotated CDS (Figures 4D). Consistently, we found

188 that transcripts related to neuronal functions typically contain long 5′ UTR and many upstream
189 AUG (Figure S5). We thus propose that glial cells suppress the translation of neuronal
190 transcripts by stalling ribosomes on 5′ UTR via uORF.

191 ***Rh1* UTR confers translational suppression in glia**

192 We next asked if the UTR sequences of neuronal genes cause cell-type differences in
193 translation. To this end, we focused on *Rh1* (*Rhodopsin 1*, also known as *ninaE*). The Rh1
194 protein, the opsin with a broadband spectral sensitivity, is heavily expressed in the
195 photoreceptor neurons, and is also responsible for detecting stimuli of other sensory modalities
196 (32–35). Accordingly, TE of *Rh1* in neurons was 13.5 times as high as that in glial cells (Figure
197 S3B). Ribosome footprints on the *Rh1* transcript were heavily biased to 5′ UTR in glia, with the
198 striking accumulation on the putative uORFs composed only of the start and stop codons
199 (Figure 5A).

200 We constructed a transgenic reporter strain using the *Rh1* UTR sequences under the
201 control of UAS (Figure 5B), and directed gene expression ubiquitously using *Tub-GAL4*. The
202 reporter mRNA was detected both in neurons and glial cells. On the other hand, the protein
203 levels were much more heterogeneous and strikingly weak in glia than in neurons (Figure 5C).
204 Driving the reporter expression using the *nSyb*- or *repo-GAL4* driver further corroborated cell-
205 type specific suppression in glia (Figure S6). This post-transcriptional difference between the
206 cell types was in stark contrast to the control reporter strain (36), which were expressed both
207 in neurons and in glia (Figure 5C). Based on these results, we propose that glial cells
208 selectively suppress the protein synthesis of neuronal genes through the UTR sequence and
209 thereby enhance the translatome distinction from neurons.

210

211 **Discussion:**

212 The comparative translatome-transcriptome analyses in the whole heads, neurons and
213 glial cells revealed the significant diversity of translational regulations across different cell
214 types. Particularly noteworthy was the differential translation of transcripts encoding neuronal
215 proteins, including ion channels and neurotransmitter receptors (Figure 2). These transcripts
216 exhibited preferential translation in neurons (Figure 2), and the relatively long 5′ UTR of these
217 transcripts strongly stalled ribosomes in glia (Figures 3, S5). While the 5′ UTR-mediated
218 translational regulations are known to be critical for quick response to environmental changes,
219 such as starvation or oxidative stress (37–39), our study sheds light on its roles in contrasting
220 protein expression among cell types. Furthermore, considering a pivotal role of *de novo* protein

221 synthesis for long-lasting adaptation (40,41), it is plausible that similar mechanisms are
222 employed for neuronal plasticity as well. Since several proteins, such as eIF1, MCT-1/DENR,
223 eIF3, and eIF2α kinases, were reported to regulate the rate of translation of uORF or re-
224 initiation after uORFs (42–45), similar molecular machineries might also be recruited for the
225 cell-type distinctions at translation. Given that long 5′ UTRs containing numerous uORFs are
226 also a characteristic feature of neuronal transcripts in mammals (46), it is likely that these
227 regulatory mechanisms are evolutionarily conserved.

228 Our cell-type specific translatome analysis further revealed translational regulations
229 beyond 5′ UTR. We found a remarkable ribosomal stall at the initiation codon in several
230 transcripts, a phenomenon observed in neurons but not in the entire heads (Figure S3). These
231 transcripts are known to be massively expressed in the fat bodies but less in the nervous
232 system (28,29), and the translation was further suppressed in neurons (Figure S3). Therefore,
233 transition from initiation to elongation may serve as another regulatory checkpoint of protein
234 synthesis (47,48), which enhances cell-type distinctions. Furthermore, we found ribosome
235 footprints also on the 3′ UTR of certain transcripts, such as *Synapsin* (Figure 3C). Stop-codon
236 readthrough has been reported to be more frequent in neurons than in other cell types (49–
237 51). Because the readthrough events extend the protein C-terminus, its regulation can add yet
238 another layer of cell-type diversity (14,52,53). Altogether, we here propose that translational
239 regulations further differentiate transcriptome distinctions, thereby shaping the cellular identity.

240 Due to the specialized functions of neuronal and glial cells, they express distinct sets of
241 proteins. Neurons allocate more ribosomes to proteins related to neurotransmission, visual
242 sensing and oxidative phosphorylation, while glial cells synthesize transporters and enzymes
243 for metabolism of amino acid, fatty acid or carbohydrates (Figure S1F). Despite these clear
244 differences and specialization, a significant amount of neuronal and glial cells has a common
245 developmental origin. They originate from a stem cell lineage known as neuro-glioblasts
246 (54,55), and the fate of these cells can be altered by the expression of a single gene, *glial cells*
247 *missing* (*gcm*) (10,56). Therefore, translational regulations may play a particularly important
248 role in these sister cell types with distinct physiological roles.

249 In the *Drosophila* brain, approximately 100 stem cell lineages diverge into more than
250 5,000 morphologically distinct cell types (6,57,58). Hence, translational regulations similar to
251 those described in this study, or other possible regulations, may play significant roles in further
252 differentiating neuronal or glial subtypes. Consistent with this idea, our *UAS-Rh1-Venus*
253 reporter showed heterogeneous expression even among neurons (Figures 5C, S6). Similarly,

254 choline acetyltransferase (ChAT), an enzyme needed to synthesize acetylcholine, is
255 transcribed in many glutamatergic and GABAergic neurons but its protein synthesis is inhibited
256 at the level of translation (59). Altogether, comparative translatome in diverse cell types using
257 more specific GAL4 drivers should highlight the diversity of post-transcriptional regulations
258 leveraged in the brain.

259

260 **Materials and Methods:**

261 **Fly culture and genetics**

262 The flies were reared in a mass culture at 24 ºC under the 12-12 hour light-dark cycles on
263 the standard cornmeal food. The *Canton-S* strain was used as the wild-type. We utilized the
264 following transgenic strains: *w^{1118};;GMR57C10-GAL4* (*nSyb-GAL4*; BDSC #39171),
265 *w^{1118};;repo-GAL4* (BDSC #7415), *y^1w^{1118};;tublin-GAL4* (BDSC #5138), *w^{1118};;UAS-*
266 *RpL3::FLAG* (BDSC #77132) (18), *y^1v^1;UAS-Rh1-Venus* (made in this study; see below),
267 *w;UASz-GFP* (a kind gift from Dr. Steven DeLuca) (36). Females of the GAL4 drivers were
268 crossed to males of the UAS effectors, and the F1 progenies were used for the experiments.
269 Of note, although *UAS-EGFP::RpL10Ab* (22) has been used to isolate ribosomes from specific
270 cells, its expression using the *repo-GAL4* caused lethality in our hands (data not shown).

271 **Library preparation for ribosome profiling**

272 *Tissue collection and lysate preparation*

273 Four to eight days old flies with mixed gender were flash-frozen with liquid nitrogen,
274 thoroughly vortexed, and the heads were isolated from the bodies with metal mesh in a similar
275 manner reported previously (60). Approximately 500 frozen heads were mixed with 400 µl of
276 frozen droplets of lysis buffer [20 mM Tris-HCl pH7.5, 150mM NaCl, 5 mM $MgCl_2$, 1 mM
277 dithiothreitol, 1 % Triton X-100, 100 µg/ml chloramphenicol, and 100 µg/ml cycloheximide] in
278 a pre-chilled container, then pulverized with grinding at 3,000 rpm for 15 seconds using a Multi-
279 beads Shocker (YASUI KIKAI). The lysate was slowly thawed at 4 °C and the supernatant was
280 recovered after spinning down by a table top micro centrifuge. The lysate was treated with 10
281 U of Turbo DNase (ThermoFisher Scientific) on ice for 10 min to digest the genome DNA. The
282 supernatant was further clarified by spinning at 20,000 g for 10 minutes.

283 *Immunoprecipitation*

284 Anti-FLAG M2 antibody (F1804, Sigma Aldrich) and Dynabeads M-280 bound to anti-
285 mouse IgG antibody (11201D, Invitrogen) were used for immunoprecipitation. 25 µl of the

286 beads solution, washed twice with the aforementioned lysis buffer, was mixed with 2.5 µl of
287 the M2 antibody, and incubated at 4 °C for 1 hour with rotation. Beads were incubated with the
288 lysate at 4 °C for 1 hour with rotation and washed for four times with the lysis buffer. The
289 ribosome-bound mRNA was eluted with 50 µl of 100 µg/ml 3× FLAG peptide (GEN-3XFLAG-
290 25, Protein Ark) dissolved in the lysis buffer.

291 *RNase digestion and library preparation*

292 Ribosome footprinting was performed as described previously (61,62) with modifications.
293 We used RNase I from *E. coli* (N6901K, Epicentre) to digest the crude (Figures 1, S1C-D) or
294 the immunoprecipitated (Figure 2) lysate. Concentration of RNA in lysate were measured with
295 Qubit RNA HS kit (Q32852, Thermo Fisher Scientific). RNase I was added at a dose of 0.25
296 U per 1 µg RNA in a 50 µl reaction and incubated at 25 °C for 45 minutes. We used 1.36 µg
297 and 0.5 µg RNA to prepare the whole head libraries (Figures 1, S1C-D) and the cell-type
298 specific libraries (Figure 2-3), respectively. The RNase digestion was stopped by adding 20 U
299 of SUPERase•In (AM2694, ThermoFisher Scientific). Ribosomes were isolated by MicroSpin
300 S-400 HR columns (27-5140-01, GE Healthcare). Subsequently, we purified RNA using the
301 TRIzol-LS (10296010, ThermoFisher Scientific) and Direct-zol RNA Microprep kit (R2062,
302 Zymo Research), and isolated the RNA fragment ranging 17 to 34 nt by polyacrylamide gel
303 electrophoresis.

304 The isolated RNA fragments were ligated to custom-made preadenylated linkers
305 containing unique molecular identifiers and barcodes for library pooling, using T4 RNA ligase
306 2, truncated KQ (M0373L, New England Biolabs) (62). Ribosomal RNA was depleted by
307 hybridizing to the custom-made biotinylated 2′-*O*-methyl oligonucleotides with complementary
308 sequences to the *Drosophila* rRNA (see *Supporting Information Text* for the sequences), which
309 can be pulled-down using the streptavidin-coated beads (65001, ThermoFisher Scientific). The
310 rRNA-depleted samples were reverse-transcribed with ProtoScript II (M0368L, New England
311 Biolabs), circularized with CircLigase II (CL9025K, Epicentre), and PCR-amplified using
312 Phusion polymerase (M0530S, New England Biolabs) (62). The libraries were sequenced with
313 the Illumina HiSeq 4000 system (Illumina) with an option of single end reads for 50 bases.

314 **Library preparation for transcriptome analysis**

315 The crude (Figure 1) or the immunoprecipitated (Figure 2) lysate was prepared using the
316 same protocol as described above, but without RNase digestion. RNA was purified using
317 TRIzol-LS. The libraries were constructed in Azenta Japan Corporation, using the NEBNext
318 Poly(A) mRNA Magnetic Isolation Module (E7760, New England Biolabs) and MGIEasy RNA

319 Directional Library Prep kit (1000006386, MGI tech). Briefly, poly-A tailed mRNAs were
320 enriched with the oligo dT beads, fragmented, and reverse-transcribed using random primers.
321 After the second strand cDNA was synthesized, an adapter sequence was added. DNA library
322 was PCR-amplified. The libraries were sequenced with DNB-seq (MGI tech) with an option of
323 paired end reads for 150 bases.

324 **Data analysis**

325 Adaptor sequences were removed using Fastp (63), and the reads that matched to the
326 non-coding RNA were discarded. The remaining reads were mapped onto the *Drosophila*
327 *melanogaster* release 6 genome. Mapping was performed using STAR (64). PCR-duplicated
328 reads were removed by referring to the unique molecular identifiers. The number of uniquely
329 mapped reads are as follows:

330 Ribo-seq:

Sample	#Reads
Canton-S, whole heads	1,427,090
nSyb-GAL4/UAS-RpL3::FLAG, after IP, replicate 1	2,443,467
nSyb-GAL4/UAS-RpL3::FLAG, after IP, replicate 2	1,135,284
repo-GAL4/UAS-RpL3::FLAG, after IP, replicate 1	2,698,259
repo-GAL4/UAS-RpL3::FLAG, after IP, replicate 2	2,133,920
nSyb-GAL4/UAS-RpL3::FLAG, whole heads, replicate 1	2,147,092
nSyb-GAL4/UAS-RpL3::FLAG, whole heads, replicate 2	2,361,588
repo-GAL4/UAS-RpL3::FLAG, whole heads, replicate 1	1,372,502
repo-GAL4/UAS-RpL3::FLAG, whole heads, replicate 2	1,846,122

331

332 RNA-seq:

Sample	#Reads
Canton-S, whole heads	29,132,939
nSyb-GAL4/UAS-RpL3::FLAG, after IP, replicate 1	40,638,850
nSyb-GAL4/UAS-RpL3::FLAG, after IP, replicate 2	34,247,848
repo-GAL4/UAS-RpL3::FLAG, after IP, replicate 1	30,906,375

repo-GAL4/UAS-RpL3::FLAG, after IP, replicate 2 31,928,337

333

334 For Ribo-seq analysis, fragments ranging from 20 to 34 nt for whole head samples and
335 21 to 36 nt for immunoprecipitated samples were used. For the whole head samples, the
336 position of the P site was estimated as 12 or 13 nt downstream from the 5′ end, for the 20 to
337 31 nt or 32-34 nt fragments, respectively (11). For the immunoprecipitated samples, it was
338 estimated as 12 or 13 nt downstream for the 21 nt or 22-36 nt fragments, respectively.
339 Footprints were considered to be on the CDS if the estimated P site was between the
340 annotated start and stop codons. RNA-seq analysis included all fragments greater than 30 nt
341 in length. For genes with alternatively spliced transcripts, the isoform with the highest TPM in
342 the wild type RNA-seq sample (Figure 1) was selected as the 'representative' isoform. If not
343 specified, only the representative isoforms were considered. TE was calculated as TPM of
344 ribosome footprints on CDS divided by TPM of RNA-seq.

345 The KEGG-enrichment analyses were performed using iPAGE (Figures 1H and 2D) (65)
346 or DAVID (Figures S1F and S3A) (66). Statistical tests were performed with GraphPad Prism
347 9.

348 **Reporter construct and the transgenic strain**

349 A DNA fragment containing a minimal hsp70 promoter (hsp70Bb) (36), the 5′ UTR and
350 the first 15 bases of the CDS of *Rh1-RA*, the Venus yellow fluorescent protein gene, and the
351 3′ UTR of *Rh1-RA* was synthesized and cloned into the pBFv-UAS3 plasmid (Addgene
352 #138399). The sequence of the resultant plasmid is provided in the *Supporting Information*
353 *Text*. The plasmid was then injected into y^1 v^1 *P{nos-phiC31}; P{CaryP}attP40,* and their
354 progenies were screened for a *v*+ phenotype. A single transformant was crossed to y^1 cho^2 v^1*;*
355 *Sp/CyO* balancer to establish a transgenic line.

356 **Immunohistochemistry and fluorescent in-situ hybridization**

357 Immunohistochemistry (Figures 2A and S1A-B) was performed as previously described
358 with minor modifications (67). Briefly, dissected male fly brains were fixed in 2 %
359 paraformaldehyde in PBS for 1 hour at room temperature, washed three times with PBST
360 (0.1 % Triton X-100 in PBS), blocked with 3 % goat serum in PBST for 30 minutes, then
361 incubated with the primary antibody solution at 4 ºC overnight (mouse anti-FLAG (1:1000;
362 Sigma-Aldrich; F1804) and rat anti-elav (1:20; DSHB; 7E8A10)). Subsequently, the brains
363 were washed for three times with PBST, incubated with the secondary antibody solution at 4

364 ºC overnight (anti-mouse Alexa Fluor 488 (1:400; Invitrogen; A11001) and anti-rat Cy3 (1:200;
365 Jackson ImmunoResearch; 112-166-003)), washed three times with PBST and mounted with
366 86 % glycerol in PBS.

367 Fluorescent in-situ hybridization, combined with immunohistochemistry, was performed in
368 a similar manner to (68) with several modifications (Figure 5C). Dissected male fly brains were
369 fixed in PBS containing 3 % formaldehyde, 1 % glyoxal and 0.1 % methanol for 30 min at room
370 temperature, followed by three quick washes with PBT (0.5 % Triton X-100 in PBS). We
371 confirmed that the addition of glyoxal to the fixative improves the FISH signal (data not shown)
372 (69). The buffer was then exchanged to the wash solution (10 % Hi-Di™ Formamide
373 (Thermofisher scientific; 4311320) in 2x saline sodium citrate (SSC)) and was incubated at 37
374 ºC for 5 minutes. Subsequently, the brains were incubated with the custom-made Stellaris
375 *Venus* or *GFP* probes (100 nM; see *Supporting Information Text* for the sequences; LGC
376 BioSearch Technologies) and the primary antibody (mouse anti-Repo (1:100; DSHB; 8D12))
377 in the hybridization buffer (10% Hi-Di™ Formamide in hybridization buffer (Stellaris RNA FISH
378 Hybridization Buffer, SMF-HB1-10)) at 37 ºC for 16 hours. The probes and the antibody were
379 then removed by washing the samples quickly three times with preheated wash solution at 37
380 ºC, followed by three washes for 10 minutes at room temperature. Blocking was performed
381 with 3 % normal goat serum in PBT for 30 min at room temperature. The secondary antibody
382 (Cy3 goat anti-mouse (1:2000; Jackson ImmunoResearch; 115-166-003)) was then added and
383 was incubated at 4 ºC overnight. The samples were washed once quickly, three times for 20
384 minutes, and once for 60 minutes with PBT, and then mounted in 86 % glycerol in 1x Tris-HCl
385 buffer (pH7.4).

386 Tissues to detect native GFP or Venus signals (Figure S6) were prepared as follows:
387 dissected brains were fixed in PBS containing 3 % formaldehyde, 1 % glyoxal and 0.1 %
388 methanol for 30 min at room temperature, followed by one quick wash and three washes for
389 10 minutes with PBT. The samples were then mounted in 86 % glycerol in 1x Tris-HCl buffer
390 (pH7.4).

391 **Imaging and microscopes**

392 Imaging was done on the Olympus FV1200 confocal microscope with GaAsP sensors. A
393 100x/1.35 silicone immersion objective (UPLSAPO100XS, Olympus) or 30x/1.05 silicone
394 immersion objective (UPLSAPO30XS) was used. Scan settings were kept constant across
395 specimens to be compared.

Acknowledgments:

We thank Dr. Steven DeLuca (Brandeis university), Dr. Atsushi Sugie (Niigata University), and Dr. Yohei Nitta (Niigata University) for kindly providing the transgenic flies. We also thank Dr. Yusuke Kimura and Dr. Yukihide Tomari (The University of Tokyo) for designing the fly rRNA-depletion probes, Ayako Abe (Tohoku University) for technical assistance, Dr. Takashi Makino (Tohoku University) for critical discussion, Madoka Ichinose for critical comments on the graphic design, and the HOKUSAI SailingShip supercomputer facility at RIKEN for computational supports.

This study was supported by the Ministry of Education, Culture, Sports, Science and Technology (MEXT): 21K06369 (to TI), 21H05713 (to TI), JP20H05784 (to SI), JP21K15023 (to YS), 22H05481 (to HT), 22KK0106 (to HT), 20H00519 (to HT); Japan Society for the Promotion of Science (JSPS): 21K06369 (to TI), JP21K15023 (to YS); Japan Agency for Medical Research and Development (AMED): JP23gm1410001 (to SI); Takeda Life Science Research Grant (to TI); RIKEN-Tohoku Univ Science & Technology Hub Collaborative Research Program (to TI and YS), “Biology of Intracellular Environments” (to SI), Special Postdoctoral Researchers (to YS), and Incentive Research Projects (to YS), Tohoku University Research Program “Frontier Research in Duo” (to HT).

415 **References:**

416 1. Schwanhäusser B, Busse D, Li N, Dittmar G, Schuchhardt J, Wolf J, et al. Global
417 quantification of mammalian gene expression control. Nature. 2011 May
418 19;473(7347):337–42.

419 2. Liu Y, Beyer A, Aebersold R. On the Dependency of Cellular Protein Levels on
420 mRNA Abundance. Cell. 2016 Apr;165(3):535–50.

421 3. Casas-Vila N, Bluhm A, Sayols S, Dinges N, Dejung M, Altenhein T, et al. The
422 developmental proteome of *Drosophila melanogaster*. Genome Res. 2017
423 Jul;27(7):1273–85.

424 4. Becker K, Bluhm A, Casas-Vila N, Dinges N, Dejung M, Sayols S, et al.
425 Quantifying post-transcriptional regulation in the development of Drosophila
426 melanogaster. Nat Commun. 2018 Nov 26;9(1):4970.

427 5. Li J, Han S, Li H, Udeshi ND, Svinkina T, Mani DR, et al. Cell-Surface
428 Proteomic Profiling in the Fly Brain Uncovers Wiring Regulators. Cell. 2020
429 Jan;180(2):373-386.e15.

430 6. Scheffer LK, Xu CS, Januszewski M, Lu Z, Takemura S ya, Hayworth KJ, et al.
431 A connectome and analysis of the adult Drosophila central brain. eLife. 2020 Sep
432 7;9:e57443.

433 7. Davie K, Janssens J, Koldere D, De Waegeneer M, Pech U, Kreft Ł, et al. A
434 Single-Cell Transcriptome Atlas of the Aging Drosophila Brain. Cell. 2018
435 Aug;174(4):982-998.e20.

436 8. Li H, Janssens J, De Waegeneer M, Kolluru SS, Davie K, Gardeux V, et al. Fly
437 Cell Atlas: A single-nucleus transcriptomic atlas of the adult fruit fly. Science. 2022 Mar
438 4;375(6584):eabk2432.

439 9. Croset V, Treiber CD, Waddell S. Cellular diversity in the Drosophila midbrain
440 revealed by single-cell transcriptomics. eLife. 2018 Apr 19;7:e34550.

441 10. Hartenstein V. Morphological diversity and development of glia in *Drosophila*.
442 Glia. 2011 Sep;59(9):1237–52.

443 11. Ingolia NT, Ghaemmaghami S, Newman JRS, Weissman JS. Genome-wide
444 analysis in vivo of translation with nucleotide resolution using ribosome profiling.
445 Science. 2009 Apr;324(5924):218–23.

446 12. Ingolia NT, Lareau LF, Weissman JS. Ribosome Profiling of Mouse Embryonic
447 Stem Cells Reveals the Complexity and Dynamics of Mammalian Proteomes. Cell. 2011
448 Nov;147(4):789–802.

449 13. Zhang H, Dou S, He F, Luo J, Wei L, Lu J. Genome-wide maps of ribosomal
450 occupancy provide insights into adaptive evolution and regulatory roles of uORFs during
451 Drosophila development. Chen X, editor. PLoS Biol. 2018 Jul 20;16(7):e2003903.

452 14. Dunn JG, Foo CK, Belletier NG, Gavis ER, Weissman JS. Ribosome profiling
453 reveals pervasive and regulated stop codon readthrough in Drosophila melanogaster.
454 eLife. 2013 Dec 3;2:e01179.

455 15. Fujii K, Shi Z, Zhulyn O, Denans N, Barna M. Pervasive translational regulation
456 of the cell signalling circuitry underlies mammalian development. Nat Commun. 2017
457 Feb 14;8(1):14443.

458 16. Wang H, Wang Y, Yang J, Zhao Q, Tang N, Chen C, et al. Tissue- and stage-
459 specific landscape of the mouse translatome. Nucleic Acids Research. 2021 Jun
460 21;49(11):6165–80.

461 17. Kremer MC, Jung C, Batelli S, Rubin GM, Gaul U. The glia of the adult
462 *Drosophila* nervous system: Glia Anatomy in Adult Drosophila Nervous System. Glia.
463 2017 Apr;65(4):606–38.

464 18. Chen X, Dickman D. Development of a tissue-specific ribosome profiling
465 approach in Drosophila enables genome-wide evaluation of translational adaptations.
466 Desplan C, editor. PLoS Genet. 2017 Dec 1;13(12):e1007117.

467 19. You S, Yu AM, Roberts MA, Joseph IJ, Jackson FR. Circadian regulation of the
468 Drosophila astrocyte transcriptome. Ewer J, editor. PLoS Genet. 2021 Sep
469 20;17(9):e1009790.

470 20. Scheckel C, Imeri M, Schwarz P, Aguzzi A. Ribosomal profiling during prion
471 disease uncovers progressive translational derangement in glia but not in neurons. eLife.
472 2020 Sep 22;9:e62911.

473 21. Sapkota D, Lake AM, Yang W, Yang C, Wesseling H, Guise A, et al. Cell-Type-
474 Specific Profiling of Alternative Translation Identifies Regulated Protein Isoform
475 Variation in the Mouse Brain. Cell Reports. 2019 Jan;26(3):594-607.e7.

476 22. Thomas A, Lee PJ, Dalton JE, Nomie KJ, Stoica L, Costa-Mattioli M, et al. A
477 Versatile Method for Cell-Specific Profiling of Translated mRNAs in Drosophila. Roman
478 G, editor. PLoS ONE. 2012 Jul 6;7(7):e40276.

479 23. Cho J, Yu NK, Choi JH, Sim SE, Kang SJ, Kwak C, et al. Multiple repressive
480 mechanisms in the hippocampus during memory formation. Science. 2015 Oct
481 2;350(6256):82–7.

482 24. Huang K, Chen W, Zhu F, Li PWL, Kapahi P, Bai H. RiboTag translatomic
483 profiling of Drosophila oenocytes under aging and induced oxidative stress. BMC
484 Genomics. 2019 Dec;20(1):50.

485 25. Volkenhoff A, Weiler A, Letzel M, Stehling M, Klämbt C, Schirmeier S. Glial
486 Glycolysis Is Essential for Neuronal Survival in Drosophila. Cell Metabolism. 2015
487 Sep;22(3):437–47.

488 26. Mason S. Lactate Shuttles in Neuroenergetics—Homeostasis, Allostasis and
489 Beyond. Front Neurosci [Internet]. 2017 Feb 2 [cited 2023 May 10];11. Available from:
490 http://journal.frontiersin.org/article/10.3389/fnins.2017.00043/full

491 27. Singh AK. Hsrω and Other lncRNAs in Neuronal Functions and Disorders in
492 Drosophila. Life. 2022 Dec 21;13(1):17.

493 28. Dobson AJ, He X, Blanc E, Bolukbasi E, Feseha Y, Yang M, et al. Tissue-
494 specific transcriptome profiling of Drosophila reveals roles for GATA transcription
495 factors in longevity by dietary restriction. npj Aging Mech Dis. 2018 Apr 17;4(1):5.

496 29. Chintapalli VR, Wang J, Dow JAT. Using FlyAtlas to identify better Drosophila
497 melanogaster models of human disease. Nat Genet. 2007 Jun;39(6):715–20.

498 30. Ferreira JP, Overton KW, Wang CL. Tuning gene expression with synthetic
499 upstream open reading frames. Proc Natl Acad Sci USA. 2013 Jul 9;110(28):11284–9.

500 31. Zhang H, Wang Y, Lu J. Function and Evolution of Upstream ORFs in
501 Eukaryotes. Trends in Biochemical Sciences. 2019 Sep;44(9):782–94.

502 32. O'Tousa JE, Baehr W, Martin RL, Hirsh J, Pak WL, Applebury ML. The
503 Drosophila ninaE gene encodes an opsin. Cell. 1985 Apr;40(4):839–50.

504 33. Zuker CS, Cowman AF, Rubin GM. Isolation and structure of a rhodopsin gene
505 from D. melanogaster. Cell. 1985 Apr;40(4):851–8.

506 34. Shen WL, Kwon Y, Adegbola AA, Luo J, Chess A, Montell C. Function of
507 Rhodopsin in Temperature Discrimination in *Drosophila*. Science. 2011 Mar
508 11;331(6022):1333–6.

509 35. Leung NY, Thakur DP, Gurav AS, Kim SH, Di Pizio A, Niv MY, et al. Functions
510 of Opsins in Drosophila Taste. Current Biology. 2020 Apr;30(8):1367-1379.e6.

511 36. DeLuca SZ, Spradling AC. Efficient Expression of Genes in the *Drosophila*
512 Germline Using a UAS Promoter Free of Interference by Hsp70 piRNAs. Genetics. 2018
513 Jun 1;209(2):381–7.

514 37. Mueller PP, Hinnebusch AG. Multiple upstream AUG codons mediate
515 translational control of GCN4. Cell. 1986 Apr;45(2):201–7.

516 38. Harding HP, Zhang Y, Zeng H, Novoa I, Lu PD, Calfon M, et al. An Integrated
517 Stress Response Regulates Amino Acid Metabolism and Resistance to Oxidative Stress.
518 Molecular Cell. 2003 Mar;11(3):619–33.

519 39. Young SK, Wek RC. Upstream Open Reading Frames Differentially Regulate
520 Gene-specific Translation in the Integrated Stress Response. Journal of Biological
521 Chemistry. 2016 Aug;291(33):16927–35.

522 40. Tully T, Preat T, Boynton SC, Del Vecchio M. Genetic dissection of consolidated
523 memory in Drosophila. Cell. 1994 Oct;79(1):35–47.

524 41. Flexner JB, Flexner LB, Stellar E. Memory in mice as affected by intracerebral
525 puromycin. Science. 1963 Jul;141(3575):57–9.

526 42. Ivanov IP, Loughran G, Sachs MS, Atkins JF. Initiation context modulates
527 autoregulation of eukaryotic translation initiation factor 1 (eIF1). Proc Natl Acad Sci
528 USA. 2010 Oct 19;107(42):18056–60.

529 43. Sonenberg N, Hinnebusch AG. Regulation of Translation Initiation in Eukaryotes:
530 Mechanisms and Biological Targets. Cell. 2009 Feb;136(4):731–45.

531 44. Schleich S, Strassburger K, Janiesch PC, Koledachkina T, Miller KK, Haneke K,
532 et al. DENR–MCT-1 promotes translation re-initiation downstream of uORFs to control
533 tissue growth. Nature. 2014 Aug;512(7513):208–12.

534 45. Vattem KM, Wek RC. Reinitiation involving upstream ORFs regulates *ATF4*
535 mRNA translation in mammalian cells. Proc Natl Acad Sci USA. 2004 Aug
536 3;101(31):11269–74.

537 46. Glock C, Biever A, Tushev G, Nassim-Assir B, Kao A, Bartnik I, et al. The
538 translatome of neuronal cell bodies, dendrites, and axons. Proc Natl Acad Sci USA. 2021
539 Oct 26;118(43):e2113929118.

540 47. Wang J, Johnson AG, Lapointe CP, Choi J, Prabhakar A, Chen DH, et al. eIF5B
541 gates the transition from translation initiation to elongation. Nature. 2019 Sep
542 26;573(7775):605–8.

543 48. Harnett D, Ambrozkiewicz MC, Zinnall U, Rusanova A, Borisova E, Drescher
544 AN, et al. A critical period of translational control during brain development at codon
545 resolution. Nat Struct Mol Biol. 2022 Dec;29(12):1277–90.

546 49. Prieto-Godino LL, Rytz R, Bargeton B, Abuin L, Arguello JR, Peraro MD, et al.
547 Olfactory receptor pseudo-pseudogenes. Nature. 2016 Nov 3;539(7627):93–7.

548 50. Hudson AM, Szabo NL, Loughran G, Wills NM, Atkins JF, Cooley L. Tissue-
549 specific dynamic codon redefinition in *Drosophila*. Proc Natl Acad Sci USA. 2021 Feb
550 2;118(5):e2012793118.

551 51. Karki P, Carney TD, Maracci C, Yatsenko AS, Shcherbata HR, Rodnina MV.
552 Tissue-specific regulation of translational readthrough tunes functions of the traffic jam
553 transcription factor. Nucleic Acids Research. 2022 Jun 24;50(11):6001–19.

554 52. Klagges BRE, Heimbeck G, Godenschwege TA, Hofbauer A, Pflugfelder GO,
555 Reifegerste R, et al. Invertebrate Synapsins: A Single Gene Codes for Several Isoforms in
556 *Drosophila*. J Neurosci. 1996 May 15;16(10):3154–65.

557 53. Jungreis I, Lin MF, Spokony R, Chan CS, Negre N, Victorsen A, et al. Evidence
558 of abundant stop codon readthrough in *Drosophila* and other metazoa. Genome Res. 2011
559 Dec;21(12):2096–113.

560 54. Lai SL, Lee T. Genetic mosaic with dual binary transcriptional systems in
561 Drosophila. Nat Neurosci. 2006 May;9(5):703–9.

562 55. Viktorin G, Riebli N, Popkova A, Giangrande A, Reichert H. Multipotent neural
563 stem cells generate glial cells of the central complex through transit amplifying
564 intermediate progenitors in Drosophila brain development. Developmental Biology. 2011
565 Aug;356(2):553–65.

566 56. Hosoya T, Takizawa K, Nitta K, Hotta Y. Glial cells missing: A binary switch
567 between neuronal and glial determination in drosophila. Cell. 1995 Sep;82(6):1025–36.

568 57. Ito M, Masuda N, Shinomiya K, Endo K, Ito K. Systematic Analysis of Neural
569 Projections Reveals Clonal Composition of the Drosophila Brain. Current Biology. 2013
570 Apr;23(8):644–55.

571 58. Yu HH, Awasaki T, Schroeder MD, Long F, Yang JS, He Y, et al. Clonal
572 Development and Organization of the Adult Drosophila Central Brain. Current Biology.
573 2013 Apr;23(8):633–43.

574 59. Lacin H, Chen HM, Long X, Singer RH, Lee T, Truman JW. Neurotransmitter
575 identity is acquired in a lineage-restricted manner in the Drosophila CNS. eLife. 2019
576 Mar 26;8:e43701.

577 60. Sun H, Nishioka T, Hiramatsu S, Kondo S, Amano M, Kaibuchi K, et al.
578 Dopamine Receptor Dop1R2 Stabilizes Appetitive Olfactory Memory through the
579 Raf/MAPK Pathway in Drosophila. J Neurosci. 2020 Apr;40(14):2935–42.

580 61. McGlincy NJ, Ingolia NT. Transcriptome-wide measurement of translation by
581 ribosome profiling. Methods. 2017 Aug;126:112–29.

582 62. Mito M, Mishima Y, Iwasaki S. Protocol for Disome Profiling to Survey
583 Ribosome Collision in Humans and Zebrafish. STAR Protocols. 2020 Dec;1(3):100168.

584 63. Chen S, Zhou Y, Chen Y, Gu J. fastp: an ultra-fast all-in-one FASTQ
585 preprocessor. Bioinformatics. 2018 Sep 1;34(17):i884–90.

586 64. Dobin A, Davis CA, Schlesinger F, Drenkow J, Zaleski C, Jha S, et al. STAR:
587 ultrafast universal RNA-seq aligner. Bioinformatics. 2013 Jan 1;29(1):15–21.

588 65. Goodarzi H, Elemento O, Tavazoie S. Revealing Global Regulatory Perturbations
589 across Human Cancers. Molecular Cell. 2009 Dec;36(5):900–11.

590 66. Dennis G, Sherman BT, Hosack DA, Yang J, Gao W, Lane HC, et al. DAVID:
591 Database for Annotation, Visualization, and Integrated Discovery. Genome Biol. 2003
592 Sep;4(9):R60.

593 67. Kanno M, Hiramatsu S, Kondo S, Tanimoto H, Ichinose T. Voluntary intake of
594 psychoactive substances is regulated by the dopamine receptor Dop1R1 in Drosophila.
595 Sci Rep. 2021 Feb 9;11(1):3432.

596 68. Yang L, Titlow J, Ennis D, Smith C, Mitchell J, Young FL, et al. Single molecule
597 fluorescence in situ hybridisation for quantitating post-transcriptional regulation in
598 Drosophila brains. Methods. 2017 Aug;126:166–76.

599 69. Yao RW, Luan PF, Chen LL. An optimized fixation method containing glyoxal
600 and paraformaldehyde for imaging nuclear bodies. RNA. 2021 Jun;27(6):725–33.

601
602

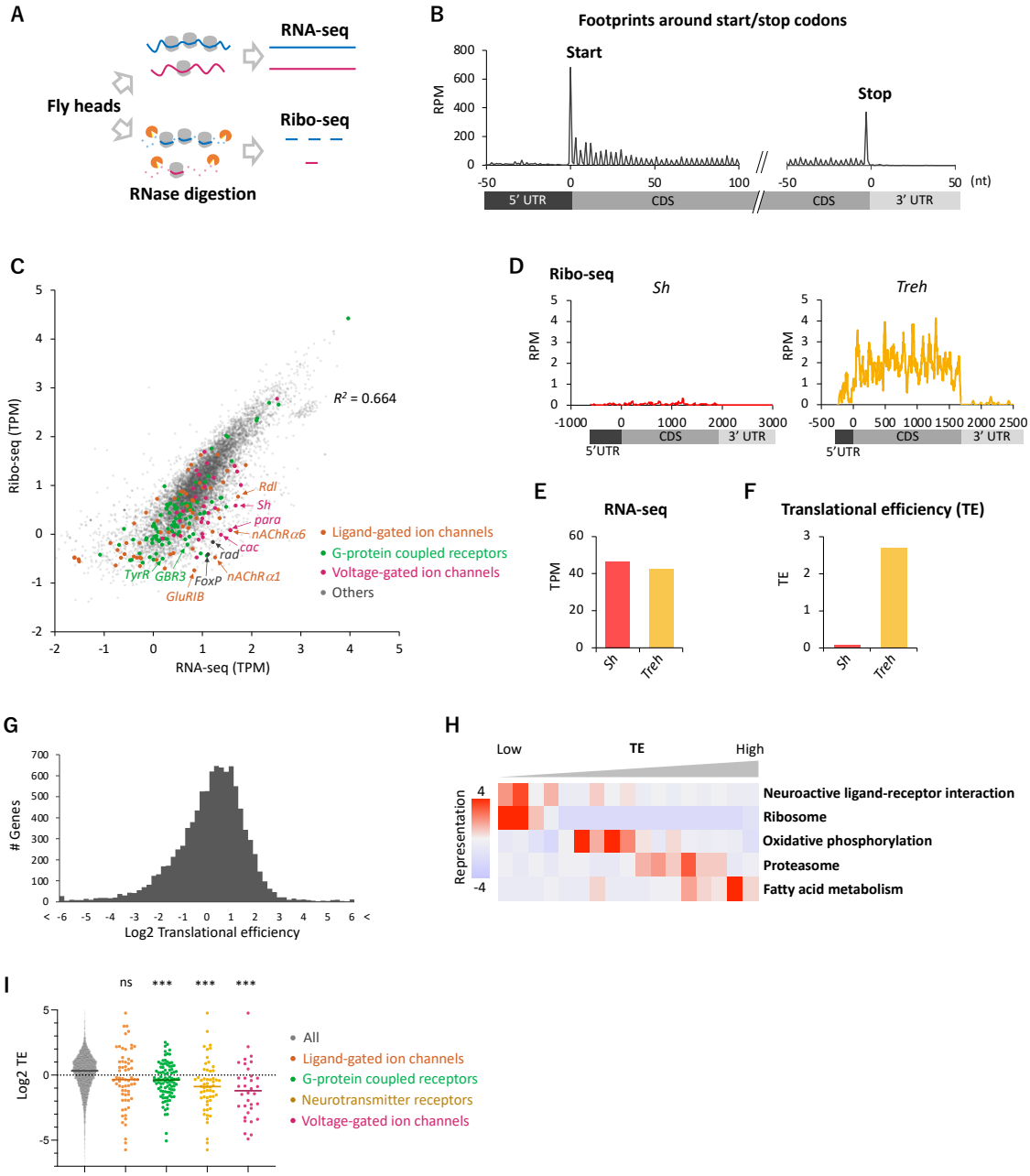

Figure 1. Comparative transcriptome-translatome analyses in the *Drosophila* head.

(*A*) Schematics. Fly head lysate is digested with RNase I for Ribo-seq, while not for RNA-seq. Resultant short fragments or the whole mRNA are reverse-transcribed and sequenced. (*B*) Meta-genome ribosome distribution (estimated P-sites of the 21-nt fragments), relative to the annotated start and stop codons. RPM: reads per million. (*C*) Scatter plots of mRNA reads (x-axis, TPM: transcripts per million) and ribosome footprints on CDS (y-axis, TPM). Several neuron-related genes are highlighted with colors and arrows. The squared Pearson's

correlation coefficient (R^2) is indicated. (*D-F*) Ribosome footprints (D), mRNA level (E), and translational efficiency (F) of *Shaker-RB* (*Sh*) and *Trehalase-RA* (*Treh*). TE: translational efficiency. TE is calculated as ribosome footprints on CDS (TPM) divided by the mRNA level (TPM). (*G*) Histogram of TE. The bin size is 0.2 in the unit of log 2. Total 9,611 genes with at least one read in both Ribo-seq and RNA-seq are plotted. (*H*) Kyoto Encyclopedia of Genes and Genomes (KEGG) pathways enrichment analysis, visualized by iPAGE (65), based on TE. The 9,611 genes are ranked and binned according to TE (left to right: low to high), and over- and under- representation is tested. The presented KEGG pathways show *P* values smaller than 0.0005. (*I*) TE of transcripts in the denoted gene ontology terms. Bars represent the median. ns: $P > 0.05$; ***: $P < 0.001$; in the Dunn's multiple comparisons test, compared to the "all" group.

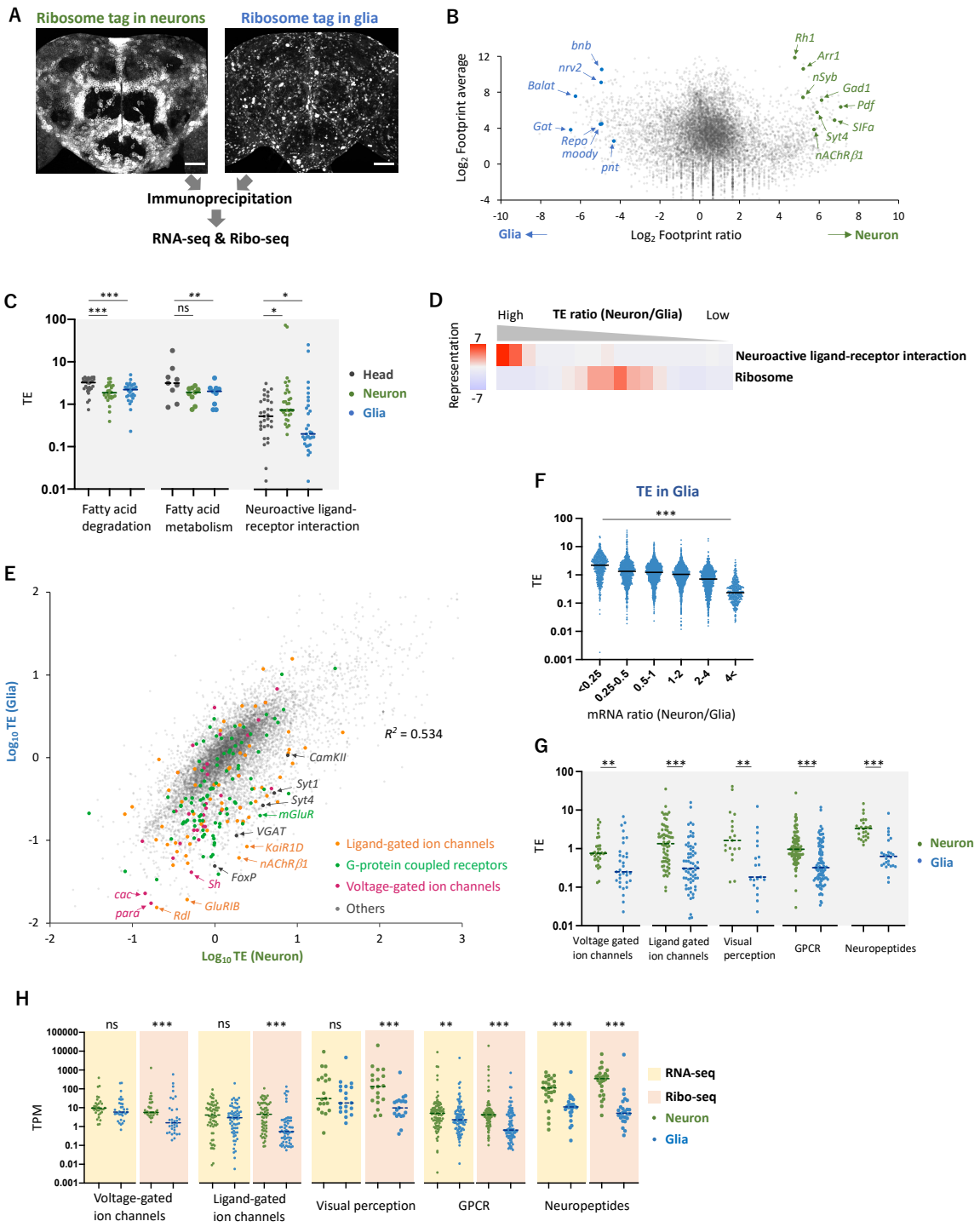

Figure 2. Cell-type specific Ribo-seq and RNA-seq reveal differential translational regulations.

(*A*) Schematics. FLAG-tagged ribosome protein L3 (RpL3::FLAG) is expressed in neurons (*nSyb-GAL4*) or in glial cells (*repo-GAL4*). RNA-seq and ribo-seq are performed following

628 immunoprecipitation. Whole brain images of the exogenously expressed RpL3::FLAG are
629 shown. Scale bars: 50 μm. (*B*) The MA-plot of ribosome footprints on CDS among neurons
630 and glia. Each gene is plotted according to the fold change (x-axis) and the average (y-axis)
631 in the unit of $\log_2$. Several marker genes are highlighted with green (neuron) or blue (glia). (*C*)
632 TE of genes in the denoted KEGG pathways in the whole head (black), neurons (green), or in
633 glia (blue). Genes with TPM > 1 in the RNA-seq dataset are plotted. Bars represent the
634 median. *: $P < 0.05$, **: $P < 0.01$, ***: $P < 0.001$, the Dunn's multiple comparisons test. (*D*)
635 KEGG pathway enrichment analysis based on the ratio of TE in neurons to in glia. All genes
636 with at least one read in both cell types (total 9,732 genes) are ranked and binned according
637 to the neuron-to-glia ratio (left to right: high to low), and over- and under- representation is
638 tested. The presented KEGG pathways show *P* values smaller than 0.0005. (*E*) Scatter plot of
639 TE in neurons (x-axis) and in glia (y-axis). The squared Pearson's correlation coefficient (R^2)
640 is indicated. (*F*) TE in glia plotted according to the ratio of mRNA expression in neurons
641 compared to glia. ***: $P < 0.001$, Kruskal-Wallis test. (*G*) TE of transcripts in the indicated gene
642 ontology (GO) terms. Bars represent the median. **: $P < 0.01$, ***: $P < 0.001$, Mann-Whitney
643 test of ranks. (*H*) Read counts of genes (TPM) in the indicated GO terms in RNA-seq (yellow)
644 and in ribo-seq (pink). The green and blue dots indicate the read counts in neuronal and glial
645 cells, respectively. ns: $P > 0.05$, **: $P < 0.01$, ***: $P < 0.001$, Mann-Whitney test of ranks.
646

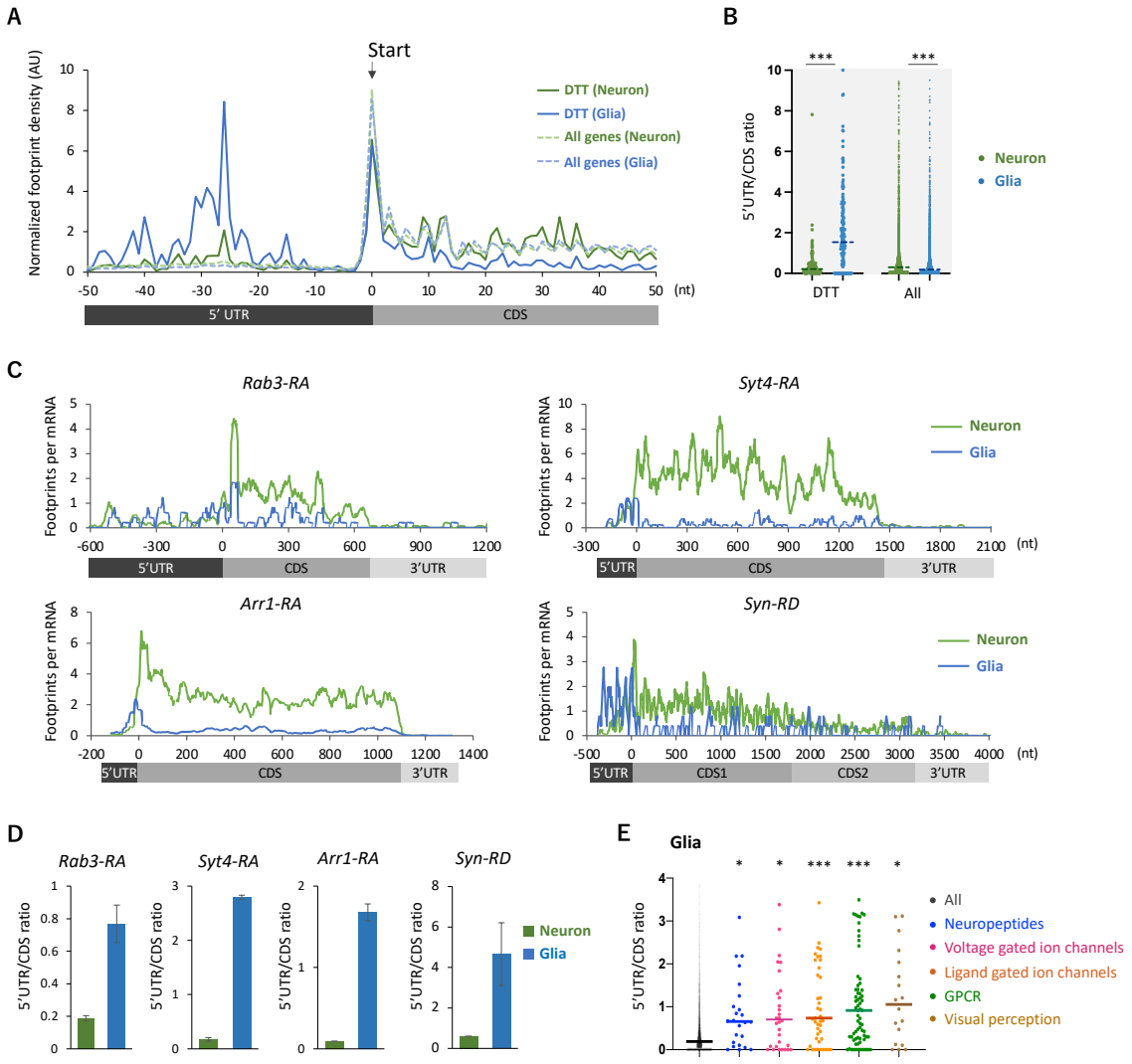

Figure 3. Ribosome stalling on the 5′ UTR of DTTs in glia.

(*A*) Ribosome distribution (estimated P-sites) on the 161 DTTs around the start codons (solid lines; start +/- 50 nt). These DTTs are defined as transcripts showing more than 10 times higher TE in neurons compared to glia. The dotted lines indicate the genome-wide distribution. Only transcripts showing TPM > 1 in RNA-seq both in neurons and glia are considered (7,933 genes in total), and the height is normalized by the total reads on this region. (*B*) Ratio of ribosome density on 5′ UTR (TPM) to CDS (TPM) of the 161 DTTs or of all transcripts in neurons (green) or in glia (blue). The bars represent the median. ***: $P < 0.001$, Mann-Whitney test of ranks. (*C*) Distribution of ribosome footprints on the representative neuronal transcripts. Ribosome footprints (RPM) normalized by the mRNA level (TPM) are shown. Note that *Syn-RD* harbors a stop codon in the CDS but a fraction of ribosomes skip it, generating two

659 annotated ORFs (CDS1 and CDS2) (52). (*D*) Ratio of ribosome density on 5′ UTR to CDS
660 (mean ± standard error of mean of the biological replicates). (*E*) Ratio of ribosome density on
661 5′ UTR to CDS on transcripts in the indicated GO terms in glia. *: $P < 0.05$, ***: $P < 0.001$,
662 Dunn's multiple comparisons test compared to the "all" group.
663

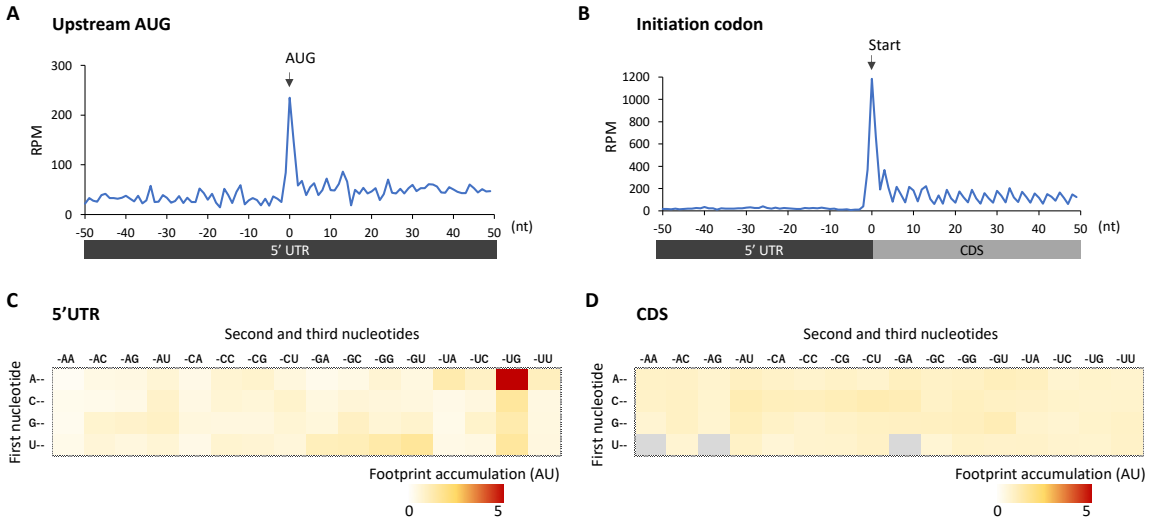

Figure 4. Footprint accumulation on upstream AUG in glia.

(*A*) Meta-genome ribosome distribution (estimated P-sites of the 32-nt fragments) around the upstream AUG codons in glia. (*B*) Meta-genome ribosome distribution (estimated P-sites of the 32-nt fragments) around the annotated start codons in glia. (*C*) Footprint accumulation on 5′ UTR in glia, defined as the number of ribosome footprints (estimated P-sites) on each codon normalized by the average on the surrounding (-50 to +50) regions. (*D*) Footprint accumulation inside the annotated CDS in glia. Annotated in-frame codons except the start and the stop codons are considered. AU: arbitrary unit.

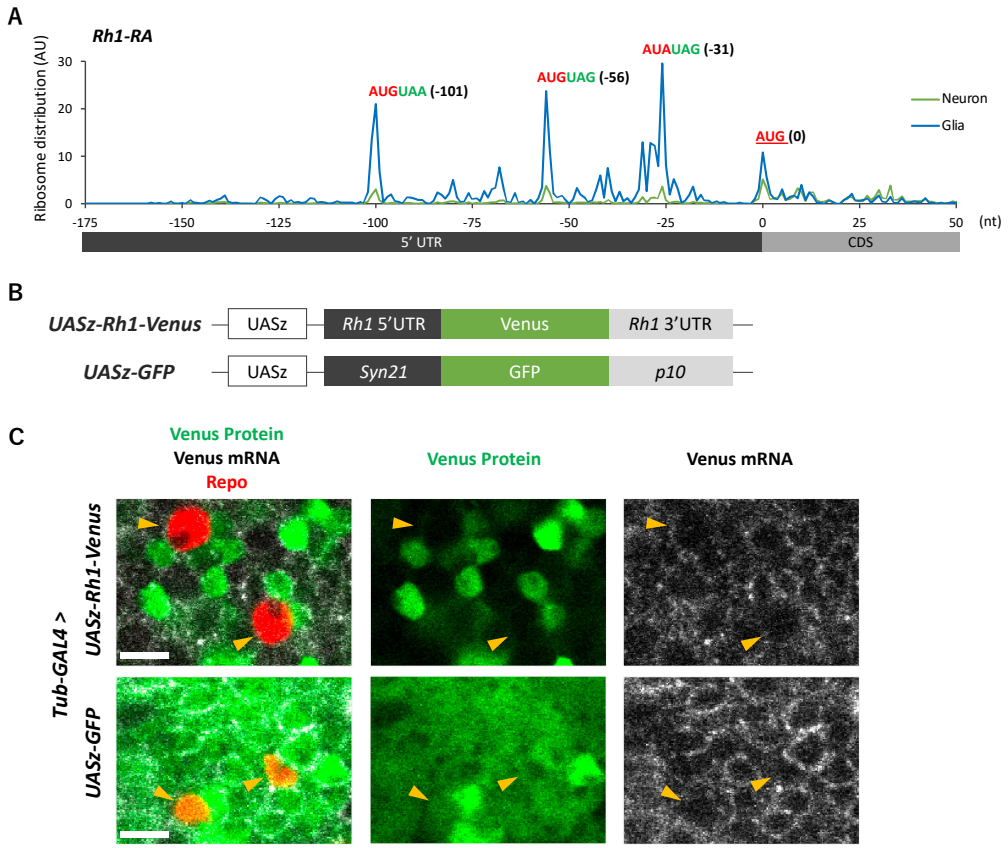

Figure 5. The transgenic *Rh1-Venus* reporter reveals differential translation in neuronal and glial cells.

(*A*) Ribosome distribution (estimated P-sites) on *Rh1-RA* in neurons (green) and in glia (blue), with 0 on the x-axis indicating the start codon of the CDS. 6-base upstream ORFs, consisting of consecutive start (or the near-cognate) and stop codons, are highlighted. Footprints are normalized by the total read counts on the transcript in each cell type. (*B*) Schematics of the *Rh1* (*UASz-Rh1-Venus*) or the control (*UASz-GFP*) reporter. For the *Rh1* reporter, 5' UTR and 3' UTR sequences of *Rh1-RA* are fused to CDS of the *Venus* fluorescent protein. For the control reporter, synthetic 5' UTR sequences (*syn21*) and viral *p10* terminator are fused to GFP (36). Note that both reporters contain the same promoter (*UASz*) (36) and are inserted onto the identical genomic locus (*attP40*). (*C*) Expression of the *Rh1*- or the control reporters driven by *Tubulin-GAL4*. Sliced confocal images of the cortical regions next to the antennal lobe are shown. Green: EGFP or Venus fluorescent signal. Red: Immunohistochemical signal of repo protein as a glial marker. Grey: EGFP or Venus mRNA. Orange arrowheads indicate glial cells marked by the repo expression. Scale bars: 5 μm.